

# From Columns to Heaps: Dimensionless Similarity with PSD-Distributed Damköhler Numbers and Dual-Porosity Flow

Juan J. Segura\*

January 22, 2026

## Abstract

This work develops a unified, dimensionless framework for comparing geometrically similar reacting porous-flow systems across scale, with emphasis on hydrometallurgical heap leaching, when particle size distribution (PSD) and intraparticle pore structure differ. Under dynamic similarity, the dimensionless liquid residence-time distribution (RTD) is identical, but differences in PSD and internal porosity break microscopic similarity. Using the shrinking-core model (SCM), the analysis shows how a PSD in particle diameter maps to a distribution of particle-scale Damköhler numbers that governs heap-averaged conversion.

Explicit PSD to Damköhler transformations are derived for (i) external film control, (ii) intraparticle diffusion control, and (iii) mixed control via additive rates. Dual-porosity hydrology relevant to sedimentary or strongly stratified ores is then incorporated by coupling SCM kinetics to mobile and immobile liquid domains, introducing additional dimensionless groups that describe interporosity exchange. Two numerical examples map a lognormal PSD into film- and diffusion-controlled Damköhler distributions and compare column/heap conversion for different PSDs. A practical workflow is outlined for hydrometallurgical column-test interpretation,

---

\*Universidad Andres Bello, Chile, juan.segura.f@unab.cl

combining tracer RTD calibration with PSD-aware kinetic fitting in dimensionless time. The framework clarifies why diffusion-controlled leaching is far more sensitive to PSD tails and dual-porosity structure than film-controlled leaching, and it identifies the compact set of dimensionless groups that must be matched to ensure similarity between laboratory columns and industrial heaps.

## 1 Introduction

Heap leaching is a key unit operation in the hydrometallurgical processing of copper, gold, uranium and other commodities, and is likely to remain so as lower-grade and more complex ores are brought into production [Dixon and Petersen, 2003, 2004, Dixon et al., 2021]. Industrial heaps are large, highly heterogeneous systems in which chemistry, flow and transport interact over a wide range of time and length scales. Despite the advances of the last two decades in column testing, 1D and 2D modelling, and field monitoring, scale-up from laboratory columns and on-off pads to multi-lift commercial heaps still relies heavily on engineering judgement and empirical factors [Dixon, 2003, ElGhamrawy et al., 2022, Robertson, 2017, Miao et al., 2017, Blackmore et al., 2018].

Two aspects are particularly important in practice. First, the hydrodynamics of drip-irrigated heaps—including unsaturated flow, channeling, and dual-porosity behaviour—control the residence time distribution (RTD) of the leaching solution, the extent of ponding and saturation, and the degree to which the solution actually contacts reactive mineral surfaces [Dixon, 2003, McBride et al., 2018, Rodrigues et al., 2023, Robertson, 2017, Miao et al., 2017, 2021]. Second, the mineral itself is distributed among a range of particle sizes and internal pore structures. The particle size distribution (PSD), internal porosity and the presence of product layers within particles jointly determine which rate-controlling mechanisms (external mass transfer, intraparticle diffusion, or surface reaction) are most important, and how much of the mineral becomes effectively “locked” in diffusion-limited domains [Szekely et al., 1975, Fuerstenau, 2005, Fogler, 2005, Moreno-Pulido et al., 2025].

Most mechanistic heap-leach models developed for hydrometallurgical systems incor-

porate some combination of advection–dispersion flow, dual-porosity or dual-permeability structure, and shrinking-core or related intraparticle kinetics [Dixon and Petersen, 2003, 2004, Dixon et al., 2021, Robertson, 2017, Miao et al., 2017, 2021, ElGhamrawy et al., 2022]. These models are powerful, but their complexity can make it difficult to see clearly which dimensionless groups control behaviour, how particle-scale heterogeneities map to heap-scale responses, and what conditions must be matched between column tests and industrial heaps to ensure meaningful similarity.

The purpose of this work is to provide a compact, dimensionless framework to clarify these issues, with a focus on industrially relevant heap-leach systems. We proceed in three main steps:

1. We discuss geometric and dynamic similarity at the reactor or heap scale, and show how matching a small set of macroscopic dimensionless groups (e.g. Peclet number, capillary and Bond numbers) leads to similar dimensionless RTDs for the liquid phase in geometrically similar heaps.
2. Using the shrinking-core model (SCM), we show how a PSD induces a distribution of particle-scale Damköhler numbers under three commonly encountered regimes: external film (convection) control, intraparticle diffusion control, and mixed control. We derive explicit expressions that map a given PSD to a distribution of Damköhler numbers in each case, and we quantify how the coarse and fine tails of the PSD affect the overall kinetics.
3. We embed the SCM into a dual-porosity hydrological framework of the type used for sedimentary and strongly stratified ores [Robertson, 2017, Miao et al., 2017, 2021, Blackmore et al., 2018], and identify the additional dimensionless parameters governing exchange between mobile (advective) and immobile (stagnant or slowly flowing) liquid domains. We then illustrate the combined framework with two simple numerical examples: (i) mapping a lognormal PSD into external- and diffusion-controlled Damköhler distributions, and (ii) an illustrative column/heap example comparing heap-averaged conversion for fine and coarse PSDs under dif-

ferent rate-controlling mechanisms.

The resulting dimensionless formulation is not a replacement for detailed numerical models, but a complement. It provides a transparent language for interpreting laboratory testwork, for comparing heaps with different PSDs and internal pore structures, and for identifying which dimensionless groups must be matched to achieve physically meaningful scale-up in hydrometallurgical heap leaching.

## 2 Analysis of the problem

### 2.1 Geometric similarity, RTD and Damköhler numbers

Non-ideal reactors, including packed beds and heaps, are often described using residence time distributions  $E(t)$  and corresponding dimensionless functions [Levenspiel, 1999, Fogler, 2016, Dixon, 2003, Rodrigues et al., 2023]. For a reactor of volume  $V$  and volumetric flow  $Q$ , the mean residence time is  $\tau = V/Q$ . The dimensionless time and RTD are

$$\theta = \frac{t}{\tau}, \quad E^*(\theta) = \tau E(t). \quad (1)$$

If two reactors are geometrically similar (all length ratios are equal) and dynamically similar (e.g. same Reynolds, Froude and other relevant dimensionless numbers for the carrier fluid), then the dimensionless RTD  $E^*(\theta)$  of the fluid phase is identical in both units.

Chemical reactions introduce further dimensionless groups, notably Damköhler numbers

$$\text{Da} = \frac{\text{reaction timescale}}{\text{flow timescale}}, \quad (2)$$

and, in distributed systems, Peclet numbers comparing advection and dispersion. In heterogeneous systems, additional groups characterise intraparticle diffusion (e.g. Thiele moduli) and the relative importance of mass transfer resistances [Fogler, 2016, Szekely et al., 1975, Fogler, 2005, Moreno-Pulido et al., 2025].

## 2.2 Heap leaching as a porous reactor

Consider a heap of height  $H$ , irrigated from the top with superficial liquid flux  $q$  and porosity  $\varepsilon$ . The interstitial velocity is  $u = q/\varepsilon$ , and a natural macroscopic time scale is the advective residence time

$$\tau_{\text{heap}} = \frac{H}{u} = \frac{\varepsilon H}{q}. \quad (3)$$

We introduce dimensionless variables

$$Z = \frac{z}{H}, \quad \Theta = \frac{t}{\tau_{\text{heap}}}, \quad (4)$$

and write a standard 1D advection–dispersion equation for the reagent concentration  $C(z, t)$ ,

$$\varepsilon \frac{\partial C}{\partial t} + (1 - \varepsilon) \rho_s \frac{\partial \bar{X}}{\partial t} + u \frac{\partial C}{\partial z} = \frac{\partial}{\partial z} \left( D_{\text{ax}} \frac{\partial C}{\partial z} \right), \quad (5)$$

where  $\bar{X}(z, t)$  is the local, particle-averaged solid conversion,  $D_{\text{ax}}$  is an effective axial dispersion coefficient, and  $\rho_s$  is the solid density. The corresponding Peclet number is

$$\text{Pe}_{\text{heap}} = \frac{uH}{D_{\text{ax}}}. \quad (6)$$

For two geometrically similar heaps operated at the same  $\text{Pe}_{\text{heap}}$  and similar saturation/wetting conditions, the dimensionless RTD of the liquid phase is expected to be similar [Dixon, 2003, McBride et al., 2018, Dixon et al., 2021].

In addition to the heap-scale length  $H$ , the system includes a second length scale, the particle diameter  $d_p$ . A fundamental geometric ratio is

$$\delta = \frac{d_p}{H}, \quad (7)$$

and the heap is characterised by a PSD  $f(d_p)$ , often expressed as a volume- or mass-based probability density.

If two heaps are geometrically similar at the macroscopic level, but the PSDs differ, then microscopic similarity is broken. Even if  $\text{Pe}_{\text{heap}}$  and other heap-scale hydrodynamic

groups are matched, the intraparticle transport and reaction behaviour will differ, and so will the overall conversion.

## 3 Material and methods

### 3.1 Shrinking-core model for individual particles

We briefly recall the SCM for spherical particles, which provides a natural microscopic description for leaching and gas–solid reactions [Szekely et al., 1975, Fogler, 2005, Fuerstenau, 2005, Moreno-Pulido et al., 2025].

Consider a spherical particle of initial radius  $R_0 = d_p/2$ , density  $\rho_s$ , and reactive solid A, contacted by a reagent in the surrounding fluid at concentration  $C_\infty$ . In the classical SCM, an unreacted core of radius  $R(t)$  shrinks with time, surrounded by a product layer through which the reagent must diffuse. Depending on the relative importance of external mass transfer, intraparticle diffusion, and intrinsic interfacial reaction, different limiting regimes arise.

In the regime where external mass transfer through a fluid film controls the rate, the characteristic time scale for conversion follows

$$t_{\text{ext}}(d_p) = \frac{\rho_s d_p}{6k_f C_\infty}, \quad (8)$$

where  $k_f$  is a mass transfer coefficient.

The conversion of a single particle may be expressed as

$$x_p(d_p, t) = g_{\text{ext}}\left(\frac{t}{t_{\text{ext}}(d_p)}, C_\infty\right), \quad (9)$$

with a known function  $g_{\text{ext}}$  depending on the specific SCM formulation and reaction order.

When diffusion through the product layer is rate-limiting, the characteristic time scale is

$$t_{\text{diff}}(d_p) = \frac{\rho_s d_p^2}{6D_{\text{eff}} C_\infty}, \quad (10)$$

where  $D_{\text{eff}}$  is an effective diffusivity in the product layer. The conversion of a particle is

$$x_p(d_p, t) = g_{\text{diff}}\left(\frac{t}{t_{\text{diff}}(d_p)}, C_{\infty}\right), \quad (11)$$

with  $g_{\text{diff}}$  again determined by the SCM expressions, e.g. the well-known diffusion-controlled shrinking-core formula  $1 - 3(1 - x)^{2/3} + 2(1 - x) = \text{const} \times t$ .

Eqs. (8) and (10) exhibit the key scale dependencies:

$$t_{\text{ext}} \propto d_p, \quad t_{\text{diff}} \propto d_p^2. \quad (12)$$

Thus, for a given heap-scale time  $\tau_{\text{heap}}$ , the ratio

$$R(d_p) = \frac{t_{\text{diff}}}{t_{\text{ext}}} = \frac{K_{\text{ext}}}{K_{\text{diff}}} d_p \quad (13)$$

varies with  $d_p$ , where  $K_{\text{ext}}$  and  $K_{\text{diff}}$  are constants defined below. Small particles tend to be more affected by diffusion control, large particles by film control, and intermediate sizes may lie in a mixed regime.

### 3.2 Particle-scale Damköhler numbers and their distributions

For a heap with characteristic time  $\tau_{\text{heap}}$ , it is natural to define particle-scale Damköhler numbers for the film- and diffusion-controlled mechanisms:

$$\text{Da}_{\text{ext}}(d_p) = \frac{\tau_{\text{heap}}}{t_{\text{ext}}(d_p)} = \frac{6k_f C_{\infty} \tau_{\text{heap}}}{\rho_s} \frac{1}{d_p} = \frac{K_{\text{ext}}}{d_p}, \quad (14)$$

$$\text{Da}_{\text{diff}}(d_p) = \frac{\tau_{\text{heap}}}{t_{\text{diff}}(d_p)} = \frac{6D_{\text{eff}} C_{\infty} \tau_{\text{heap}}}{\rho_s} \frac{1}{d_p^2} = \frac{K_{\text{diff}}}{d_p^2}, \quad (15)$$

with

$$K_{\text{ext}} = \frac{6k_f C_{\infty} \tau_{\text{heap}}}{\rho_s}, \quad K_{\text{diff}} = \frac{6D_{\text{eff}} C_{\infty} \tau_{\text{heap}}}{\rho_s}. \quad (16)$$

For a given dimensionless heap time  $\Theta = t/\tau_{\text{heap}}$ , one can write

$$x_p(d_p, \Theta) = \begin{cases} g_{\text{ext}}(\Theta \text{Da}_{\text{ext}}(d_p), C_\infty), & \text{film control,} \\ g_{\text{diff}}(\Theta \text{Da}_{\text{diff}}(d_p), C_\infty), & \text{diffusion control.} \end{cases} \quad (17)$$

The heap-averaged conversion at time  $\Theta$  is then

$$X_{\text{heap}}(\Theta) = \int_0^\infty x_p(d_p, \Theta) f(d_p) dd_p, \quad (18)$$

where  $f(d_p)$  is the PSD.

Let  $f(d_p)$  be a normalised PSD,

$$\int_0^\infty f(d_p) dd_p = 1. \quad (19)$$

We wish to determine the induced probability density  $g(\text{Da})$  of a Damköhler number of interest, using change-of-variable formulas.

### 3.2.1 External film control

For external control,  $\text{Da} = \text{Da}_{\text{ext}} = K_{\text{ext}}/d_p$ , so

$$d_p = \frac{K_{\text{ext}}}{\text{Da}}, \quad \frac{dd_p}{d\text{Da}} = -\frac{K_{\text{ext}}}{\text{Da}^2}. \quad (20)$$

Thus, the pdf  $g_{\text{ext}}(\text{Da})$  is

$$g_{\text{ext}}(\text{Da}) = f\left(\frac{K_{\text{ext}}}{\text{Da}}\right) \left| \frac{dd_p}{d\text{Da}} \right| = f\left(\frac{K_{\text{ext}}}{\text{Da}}\right) \frac{K_{\text{ext}}}{\text{Da}^2}. \quad (21)$$

Even if  $f(d_p)$  is smooth and unimodal, the factor  $\text{Da}^{-2}$  can skew the Da-distribution.

### 3.2.2 Intraparticle diffusion control

For diffusion control,  $\text{Da} = \text{Da}_{\text{diff}} = K_{\text{diff}}/d_p^2$ , so

$$d_p = \sqrt{\frac{K_{\text{diff}}}{\text{Da}}}, \quad \frac{dd_p}{d\text{Da}} = -\frac{1}{2} \sqrt{\frac{K_{\text{diff}}}{\text{Da}}} \text{Da}^{-3/2}. \quad (22)$$

The pdf  $g_{\text{diff}}(\text{Da})$  becomes

$$g_{\text{diff}}(\text{Da}) = f\left(\sqrt{\frac{K_{\text{diff}}}{\text{Da}}}\right) \frac{1}{2} \sqrt{K_{\text{diff}}} \text{Da}^{-3/2}. \quad (23)$$

Here the weighting  $\text{Da}^{-3/2}$  and the square-root mapping in the argument of  $f$  make the resulting Da-distribution even more sensitive to the small-particle (large-Da) tail of the PSD than in the film-controlled case.

### 3.2.3 Mixed control (series resistances)

When both external mass transfer and intraparticle diffusion contribute significantly, the SCM becomes more complex [Szekely et al., 1975, Fogler, 2005, Moreno-Pulido et al., 2025]. For scaling and similarity arguments, a useful approximation is to treat the two mechanisms as resistances in series, with an effective characteristic time satisfying

$$\frac{1}{t_{\text{char}}} \approx \frac{1}{t_{\text{ext}}} + \frac{1}{t_{\text{diff}}}. \quad (24)$$

This leads to an effective Damköhler number

$$\text{Da}_{\text{eff}}(d_p) = \frac{\tau_{\text{heap}}}{t_{\text{char}}(d_p)} \approx \text{Da}_{\text{ext}}(d_p) + \text{Da}_{\text{diff}}(d_p) = \frac{K_{\text{ext}}}{d_p} + \frac{K_{\text{diff}}}{d_p^2}. \quad (25)$$

To construct the corresponding distribution  $g_{\text{mix}}(\text{Da})$ , we solve for  $d_p$  as a function of Da. Multiplying Eq. (25) by  $d_p^2$ ,

$$\text{Da} d_p^2 = K_{\text{ext}} d_p + K_{\text{diff}}, \quad (26)$$

so  $d_p$  satisfies a quadratic equation

$$\text{Da} d_p^2 - K_{\text{ext}} d_p - K_{\text{diff}} = 0. \quad (27)$$

The physically relevant (positive) root is

$$d_p(\text{Da}) = \frac{K_{\text{ext}} + \sqrt{K_{\text{ext}}^2 + 4K_{\text{diff}}\text{Da}}}{2\text{Da}}. \quad (28)$$

Differentiating  $\text{Da}_{\text{eff}}(d_p)$  with respect to  $d_p$  gives

$$\frac{d\text{Da}}{dd_p} = -\frac{K_{\text{ext}}}{d_p^2} - \frac{2K_{\text{diff}}}{d_p^3} = -\frac{K_{\text{ext}}d_p + 2K_{\text{diff}}}{d_p^3}, \quad (29)$$

and hence

$$\left| \frac{dd_p}{d\text{Da}} \right| = \frac{d_p^3}{K_{\text{ext}}d_p + 2K_{\text{diff}}}. \quad (30)$$

The mixed-control Damköhler pdf is therefore

$$g_{\text{mix}}(\text{Da}) = f(d_p(\text{Da})) \frac{d_p(\text{Da})^3}{K_{\text{ext}}d_p(\text{Da}) + 2K_{\text{diff}}}, \quad (31)$$

with  $d_p(\text{Da})$  given by Eq. (28).

### 3.3 Coupling shrinking-core kinetics to dual-porosity flow

Many ore bodies, particularly sedimentary or strongly stratified deposits, exhibit internal structure that naturally suggests a dual-porosity or dual-pore-system description: relatively open macropores or preferential channels that carry most of the advective flow, and a larger volume of microporous matrix where most of the mineral resides and flow is slow, diffusive, or quasi-stagnant. This picture is closely related to dual-porosity and dual-permeability models developed in petroleum and hydrogeology [Barenblatt et al., 1960, Warren and Root, 1963, Zimmerman et al., 1993, Dogru and Pruess, 2020], and has been adapted to heap leaching in 1D column models and 3D pore-scale simulations [Robertson, 2017, Miao et al., 2017, 2021, Blackmore et al., 2018, Dixon et al., 2021].

In a dual-porosity interpretation of heap leaching, the void space is partitioned into:

- a mobile (advective) domain with porosity  $\varepsilon_m$  and concentration  $C_m(z, t)$ , and
- an immobile (stagnant or slowly moving) domain with porosity  $\varepsilon_{im}$  and concentration  $C_{im}(z, t)$ ,

with  $\varepsilon_m + \varepsilon_{im} \approx \varepsilon$ . The solid is mostly associated with the immobile domain, where diffusion-controlled SCM kinetics are often most relevant.

A widely used structure for dual-porosity models in single-phase flow is to write coupled balances for  $C_m$  and  $C_{im}$  with an interporosity mass-transfer term of the form  $\alpha(C_m - C_{im})$  [Barenblatt et al., 1960, Warren and Root, 1963, Zimmerman et al., 1993, Robertson, 2017]. For a 1D heap, one may write

$$\varepsilon_m \frac{\partial C_m}{\partial t} + u \frac{\partial C_m}{\partial z} = \frac{\partial}{\partial z} \left( D_{\text{ax},m} \frac{\partial C_m}{\partial z} \right) - \alpha(C_m - C_{im}), \quad (32)$$

$$\varepsilon_{im} \frac{\partial C_{im}}{\partial t} + (1 - \varepsilon) \rho_s \frac{\partial \bar{X}}{\partial t} = \alpha(C_m - C_{im}), \quad (33)$$

where  $D_{\text{ax},m}$  is an axial dispersion coefficient in the mobile domain, and  $\alpha$  is an interporosity exchange coefficient (units of  $\text{s}^{-1}$ ).

Introducing the macroscopic time and space scales,

$$Z = \frac{z}{H}, \quad \Theta = \frac{t}{\tau_{\text{heap}}}, \quad \tau_{\text{heap}} = \frac{H}{u}, \quad (34)$$

and defining dimensionless concentrations  $\hat{C}_m = C_m/C_\infty$ ,  $\hat{C}_{im} = C_{im}/C_\infty$ , the mobile-domain balance becomes

$$\varepsilon_m \frac{\partial \hat{C}_m}{\partial \Theta} + \frac{\partial \hat{C}_m}{\partial Z} = \frac{1}{\text{Pe}_m} \frac{\partial^2 \hat{C}_m}{\partial Z^2} - \Lambda_{\text{ex}} \left( \hat{C}_m - \hat{C}_{im} \right), \quad (35)$$

with

$$\text{Pe}_m = \frac{uH}{D_{\text{ax},m}}, \quad \Lambda_{\text{ex}} = \alpha \tau_{\text{heap}}. \quad (36)$$

Similarly, the immobile-domain balance becomes

$$\varepsilon_{im} \frac{\partial \hat{C}_{im}}{\partial \Theta} + (1 - \varepsilon) \rho_s \frac{C_\infty^{-1}}{\tau_{\text{heap}}} \frac{\partial \bar{X}}{\partial \Theta} = \Lambda_{\text{ex}} \left( \hat{C}_m - \hat{C}_{im} \right). \quad (37)$$

It is common to introduce a capacity ratio

$$\omega = \frac{\varepsilon_{im}}{\varepsilon_m}, \quad (38)$$

and a dimensionless exchange Damköhler number

$$\text{Da}_{\text{ex}} = \Lambda_{\text{ex}} = \alpha \tau_{\text{heap}}. \quad (39)$$

With these definitions, Eqs. (35)–(37) show that a dual-porosity heap is characterised, at the macroscopic level, by  $\text{Pe}_m$ ,  $\omega$  and  $\text{Da}_{\text{ex}}$ , in addition to the particle-scale Damköhler numbers of Sec. 3.2.

### 3.4 Parameter-estimation workflow (illustrative example)

Although this work is primarily a similarity and scaling analysis, the same dimensionless structure supports practical parameter estimation from column tests. The objective is to infer a minimal set of *mechanistic* parameters (e.g.  $k_f$ ,  $D_{\text{eff}}$ ,  $\alpha$ ,  $D_{\text{ax}}$ ) or, equivalently, their dimensionless combinations (e.g.  $K_{\text{ext}}$ ,  $K_{\text{diff}}$ ,  $\text{Da}_{\text{ex}}$ ,  $\text{Pe}_m$ ), from tracer RTD experiments and leaching conversion data.

#### 3.4.1 Step A: Hydrodynamic calibration from RTD

A conservative tracer test provides the outlet RTD  $E(t)$ , from which the mean residence time  $\tau$  and the dimensionless RTD  $E^*(\theta) = \tau E(t)$  are computed [Levenspiel, 1999]. A 1D advection–dispersion (or dual-porosity) model is then calibrated to the tracer response to estimate hydraulic parameters:

- Single-domain: estimate  $D_{\text{ax}}$  (thus  $\text{Pe}_{\text{heap}} = uH/D_{\text{ax}}$ ).
- Dual-porosity: estimate  $(D_{\text{ax},m}, \alpha, \omega)$ , thus  $(\text{Pe}_m, \text{Da}_{\text{ex}}, \omega)$ .

This separation is useful because tracer RTD fitting is largely independent of leaching kinetics, improving identifiability.

### 3.4.2 Step B: Particle-scale kinetic calibration from leaching curves

Let  $X_{\text{heap}}(t)$  denote the measured heap-averaged solid conversion in a column (or a representative segment of a heap). Given a measured PSD  $f(d_p)$  and calibrated hydrodynamics from Step A, kinetic parameters can be inferred by minimising a least-squares objective on *dimensionless* time:

$$\min_{\mathbf{p}} \sum_{i=1}^N [X_{\text{heap}}^{\text{model}}(\Theta_i; \mathbf{p}) - X_{\text{heap}}^{\text{data}}(\Theta_i)]^2, \quad \Theta_i = t_i/\tau_{\text{heap}}, \quad (40)$$

where  $\mathbf{p}$  may be chosen as  $(k_f, D_{\text{eff}})$  or equivalently  $(K_{\text{ext}}, K_{\text{diff}})$ . Under external film control, the model depends primarily on  $K_{\text{ext}}$  through  $\text{Da}_{\text{ext}}(d_p)$  [Eq. (14)], whereas under diffusion control it depends primarily on  $K_{\text{diff}}$  through  $\text{Da}_{\text{diff}}(d_p)$  [Eq. (15)]. In mixed control, both parameters influence the fit and can be partially correlated; the distributional mapping [Eqs. (21), (23), (31)] clarifies which PSD fractions constrain which resistance.

### 3.4.3 Step C: Consistency checks and uncertainty

A practical diagnostic is to repeat the fit under (i) film-only, (ii) diffusion-only, and (iii) mixed control, and compare residual structure. For example, a persistent late-time underprediction under film-only kinetics often indicates diffusion or immobile-domain limitations, whereas early-time underprediction under diffusion-only kinetics may indicate finite external mass transfer. Uncertainty can be quantified by bootstrap resampling of the time points or by estimating the local curvature (Hessian) of the objective near the optimum, reporting confidence intervals on  $(K_{\text{ext}}, K_{\text{diff}})$  and, if dual porosity is used, on  $(\omega, \text{Da}_{\text{ex}})$ .

### 3.4.4 Workflow summary

In compact form, a recommended workflow is:

---

- (1) Measure PSD  $f(d_p)$  and column geometry/irrigation to define  $\tau_{\text{heap}}$ .
- (2) Run tracer RTD  $\Rightarrow$  fit hydrodynamics (Pe, and if needed  $\omega, \text{Da}_{\text{ex}}$ ).
- (3) Run leaching  $X_{\text{heap}}(t) \Rightarrow$  fit  $(K_{\text{ext}}, K_{\text{diff}})$  (or  $k_f, D_{\text{eff}}$ ).
- (4) Validate by predicting a second irrigation condition or a second PSD.

---

## 4 Results and discussion

### 4.1 Numerical illustrations

To illustrate the preceding framework, we present two simple numerical examples. The goal is not to fit any particular experimental system, but rather to demonstrate how the PSD and the choice of rate-controlling mechanism influence the distributions of Damköhler numbers and the heap-averaged conversion in a dimensionless setting.

#### 4.1.1 Example 1: lognormal PSD and Damköhler distributions

We consider a lognormal PSD for the particle diameter,

$$f(d_p) = \frac{1}{d_p \sigma_{\ln} \sqrt{2\pi}} \exp\left[-\frac{(\ln d_p - \mu_{\ln})^2}{2\sigma_{\ln}^2}\right], \quad (41)$$

with median  $d_{50} = 10$  mm and geometric standard deviation  $\sigma_g = \exp(\sigma_{\ln}) \approx 1.65$  ( $\sigma_{\ln} = 0.5$ ). We discretise  $d_p \in [1, 50]$  mm on a fine grid and normalise  $f(d_p)$  numerically.

We choose dimensionless constants  $K_{\text{ext}} = 10^{-4}$  and  $K_{\text{diff}} = 10^{-6}$ . For the chosen PSD, the particle-scale Damköhler numbers

$$\text{Da}_{\text{ext}}(d_p) = \frac{K_{\text{ext}}}{d_p}, \quad \text{Da}_{\text{diff}}(d_p) = \frac{K_{\text{diff}}}{d_p^2} \quad (42)$$

are of order  $10^{-3}$ – $10^{-1}$  over the size range of interest, corresponding to moderately slow reaction relative to the heap residence time. Using the change-of-variable formulas in Eqs. (21) and (23), we construct the induced pdfs  $g_{\text{ext}}(\text{Da})$  and  $g_{\text{diff}}(\text{Da})$  by mapping the  $d_p$  grid to Da and renormalising.

For these parameter values, we obtain approximate statistics

$$\langle \text{Da}_{\text{ext}} \rangle \approx 3.1 \times 10^{-2}, \quad \text{Da}_{\text{ext},5\%} \approx 4.4 \times 10^{-3}, \quad \text{Da}_{\text{ext},95\%} \approx 2.3 \times 10^{-2},$$

$$\langle \text{Da}_{\text{diff}} \rangle \approx 4.5 \times 10^{-1}, \quad \text{Da}_{\text{diff},5\%} \approx 1.9 \times 10^{-3}, \quad \text{Da}_{\text{diff},95\%} \approx 5.2 \times 10^{-2}.$$

The diffusion-controlled distribution is much more skewed than the film-controlled one: although 90% of  $\text{Da}_{\text{diff}}$  values lie between  $\approx 2 \times 10^{-3}$  and  $\approx 5 \times 10^{-2}$ , the mean is an order of magnitude larger, reflecting a long upper tail dominated by the smallest particles.

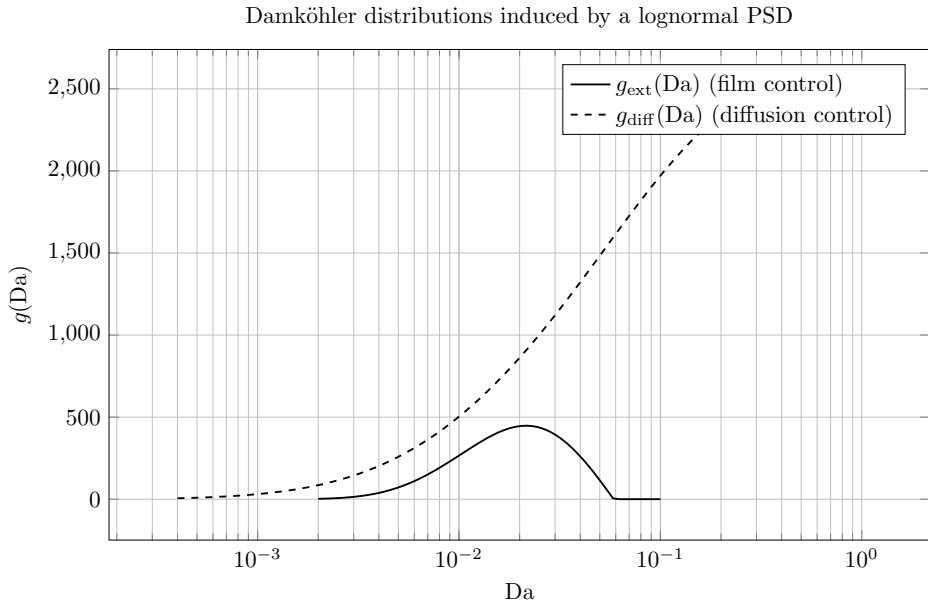


Figure 1: Damköhler distributions  $g_{\text{ext}}(\text{Da})$  and  $g_{\text{diff}}(\text{Da})$  induced by a lognormal PSD with  $d_{50} = 10$  mm and  $\sigma_{\ln} = 0.5$ , for  $K_{\text{ext}} = 10^{-4}$  and  $K_{\text{diff}} = 10^{-6}$ . The diffusion-controlled case reveals a broader, more skewed distribution with a heavier upper (high- $\text{Da}$ ) tail.

Figure 1 compares  $g_{\text{ext}}(\text{Da})$  and  $g_{\text{diff}}(\text{Da})$  on semi-logarithmic axes. The film-controlled distribution is relatively narrow, whereas the diffusion-controlled distribution exhibits a pronounced right tail. This quantitatively illustrates that, for a given PSD, diffusion-controlled kinetics are more sensitive to the presence of a fine fraction, which can dominate the overall reaction rate despite contributing a small fraction of the total solid mass.

This behaviour follows directly from the mapping  $\text{Da}_{\text{diff}} \propto d_p^{-2}$ : even a modest fine fraction translates into a disproportionately large high-Da population. As a consequence, diffusion-controlled heaps can appear kinetically “fast” at early times while simultaneously remaining sensitive to the slow leaching of coarse particles at late times, motivating explicit reporting (and, when feasible, preservation) of PSD tails in scale-up studies.

#### 4.1.2 Example 2: illustrative heap conversions for fine and coarse PSDs

As a second illustration, consider two lognormal PSDs with the same geometric standard deviation  $\sigma_{\ln} = 0.5$  but different medians: a “fine” PSD with  $d_{50} = 8 \text{ mm}$ , and a “coarse” PSD with  $d_{50} = 20 \text{ mm}$ . We again take  $K_{\text{ext}} = 10^{-4}$  and  $K_{\text{diff}} = 10^{-6}$ , and discretise  $d_p \in [1, 50] \text{ mm}$  with the same numerical resolution.

For each PSD, we compute the corresponding Damköhler numbers  $\text{Da}_{\text{ext}}(d_p)$  and  $\text{Da}_{\text{diff}}(d_p)$  and then approximate the heap-averaged conversion at dimensionless time  $\Theta$  using simple surrogate SCM-like expressions:

$$X_{\text{heap}}^{(\text{film})}(\Theta) \approx \int_0^{\infty} [1 - \exp(-\Theta \text{Da}_{\text{ext}}(d_p))] f(d_p) dd_p, \quad (43)$$

$$X_{\text{heap}}^{(\text{diff})}(\Theta) \approx \int_0^{\infty} \left[ 1 - \exp(-\Theta \sqrt{\text{Da}_{\text{diff}}(d_p)}) \right] f(d_p) dd_p. \quad (44)$$

These surrogate forms mimic the qualitative behaviour of SCM kinetics in film- and diffusion-controlled regimes while keeping the numerical example analytically simple.

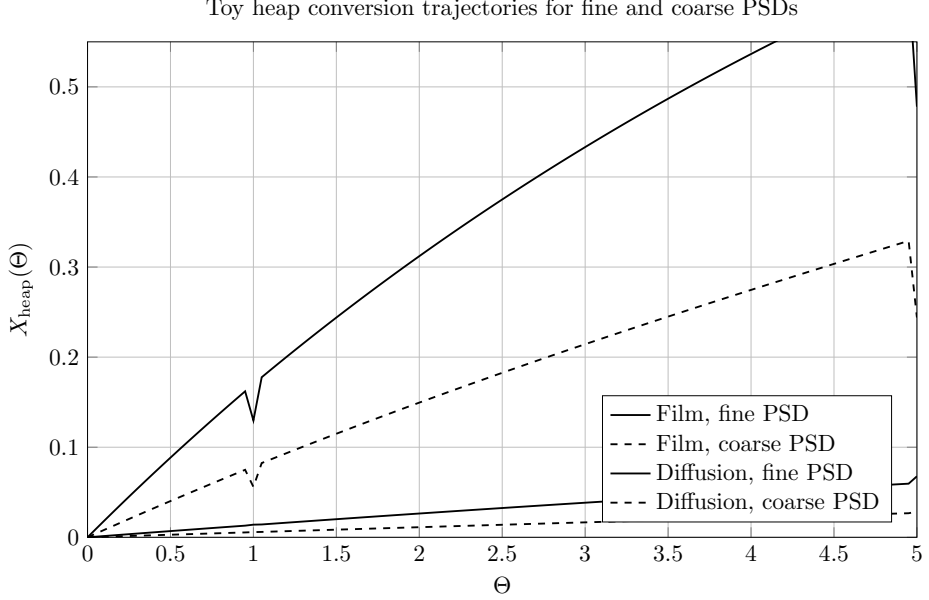


Figure 2: Heap-averaged conversion trajectories  $X_{\text{heap}}(\Theta)$  for fine ( $d_{50} = 8$  mm) and coarse ( $d_{50} = 20$  mm) PSDs under film- and diffusion-controlled surrogate kinetics [Eqs. (43)–(44)]. The diffusion-controlled cases show both higher conversions and a stronger dependence on PSD.

Figure 2 shows the resulting trajectories  $X_{\text{heap}}(\Theta)$  for  $\Theta \in [0, 5]$ . At representative times  $\Theta = 1$  and  $\Theta = 5$ , we obtain the approximate values

	$X_{\text{heap}}(\Theta = 1)$	$X_{\text{heap}}(\Theta = 5)$
Film control, fine PSD	0.014	0.068
Film control, coarse PSD	0.0058	0.028
Diffusion control, fine PSD	0.13	0.48
Diffusion control, coarse PSD	0.056	0.24

Several trends emerge:

- For both mechanisms, the fine PSD leaches faster than the coarse PSD, as expected from Eqs. (14)–(15).
- The diffusion-controlled cases show significantly higher conversions at fixed  $\Theta$  than the film-controlled cases for the chosen parameters, reflecting the larger typical  $\text{Da}_{\text{diff}}$  values.

- The *relative* penalty for coarsening the PSD is more pronounced when diffusion dominates: at  $\Theta = 5$ , the coarse-PSD conversion is about 41% of the fine-PSD value under film control and about 51% under diffusion control, but the absolute gap in  $X$  is much larger in the latter. This is consistent with the stronger  $d_p$ -dependence of  $\text{Da}_{\text{diff}} \propto d_p^{-2}$ .

A practical implication is that a single “representative” particle size is more defensible under film control than under diffusion control. When diffusion dominates, the PSD induces a broad distribution of characteristic times, so late-time recovery is governed by the coarse tail while early-time response can be dominated by fines. This separation of time scales is further amplified if dual porosity limits reagent access to the reactive matrix.

## 4.2 Similarity criteria and sensitivity to PSD and dual porosity

The expressions above allow us to state precise similarity conditions for two geometrically similar heaps, A and B, that differ in PSD and internal pore structure. Suppose that:

- The heaps have the same macroscopic geometry (same aspect ratios, slope angles, etc.).
- They are operated with the same fluid properties, reagent concentration  $C_\infty$ , and temperature.
- The macroscopic hydrodynamics are dynamically similar (same  $\text{Pe}_{\text{heap}}$  or  $\text{Pe}_m$ , similar saturation and capillary numbers).
- The dual-porosity structure is similar in the dimensionless sense ( $\omega$  and  $\text{Da}_{\text{ex}}$  matched).

Then the dimensionless RTD of the liquid phase and the partitioning between mobile and immobile domains are the same in both heaps. However, unless their *dimensionless* PSDs match (e.g. the PSD scaled by heap height,  $d_p/H$ , is identical), the distributions

of particle-scale Damköhler numbers  $g_{\text{ext}}(\text{Da})$ ,  $g_{\text{diff}}(\text{Da})$ , or  $g_{\text{mix}}(\text{Da})$ , and their ratios to  $\text{Da}_{\text{ex}}$ , will in general differ.

Because  $\text{Da}_{\text{diff}} \propto 1/d_p^2$ , diffusion-controlled heaps are significantly more sensitive to changes in PSD tails than film-controlled heaps, where  $\text{Da}_{\text{ext}} \propto 1/d_p$ . In mixed-control systems, the relative importance of film and diffusion contributions varies across the PSD, which can lead to complex responses of heap performance to changes in crushing or agglomeration practices. Dual-porosity structure further modulates this picture by controlling how effectively reagent in the mobile domain can access the immobile, reactive matrix.

From a scale-up perspective, this analysis suggests that matching only macroscopic hydrodynamic dimensionless groups is generally insufficient. For true similarity in heap leaching performance, one must also match the PSD in dimensionless form and, if possible, the distributions of relevant Damköhler numbers implied by the SCM, as well as the dual-porosity parameters  $\omega$  and  $\text{Da}_{\text{ex}}$ . This observation is consistent with more detailed, numerically intensive models of heap leaching that resolve both hydrology and intraparticle transport [Dixon and Petersen, 2003, 2004, Robertson, 2017, Miao et al., 2017, 2021, Dixon et al., 2021, ElGhamrawy et al., 2022].

Table 1: Summary of key dimensionless groups used in the analysis.

Symbol	Definition	Meaning
$Z$	$z/H$	Dimensionless vertical coordinate.
$\Theta$	$t/\tau_{\text{heap}}$	Dimensionless time.
$\delta$	$d_p/H$	Particle-to-heap size ratio.
$\varepsilon$	—	Total heap porosity.
$\varepsilon_m$	—	Mobile-domain porosity.
$\varepsilon_{im}$	—	Immobile-domain porosity.
$\omega$	$\varepsilon_{im}/\varepsilon_m$	Immobile/mobile capacity ratio.
$\text{Pe}_{\text{heap}}$	$uH/D_{\text{ax}}$	Heap Peclet number.
$\text{Pe}_m$	$uH/D_{\text{ax},m}$	Mobile-domain Peclet number.
$\text{Da}_{\text{ext}}(d_p)$	$K_{\text{ext}}/d_p$	Film-control Damköhler ( $\propto d_p^{-1}$ ).
$\text{Da}_{\text{diff}}(d_p)$	$K_{\text{diff}}/d_p^2$	Diffusion-control Damköhler ( $\propto d_p^{-2}$ ).
$\text{Da}_{\text{eff}}(d_p)$	$\approx \text{Da}_{\text{ext}} + \text{Da}_{\text{diff}}$	Effective Damköhler (mixed control).
$\text{Da}_{\text{ex}}$	$\alpha\tau_{\text{heap}}$	Mobile–immobile exchange Damköhler.

## 5 Conclusions

We developed a dimensionless framework that separates hydrodynamic similarity (from RTD/transport) from microscopic similarity (from PSD-dependent particle-scale kinetics), and shows how both must be matched for robust heap-leach scale-up. While the derivations draw on standard concepts from chemical reaction engineering, the emphasis throughout has been on quantities that are directly relevant to column testing and industrial heap design.

At the macroscopic level, we highlighted how geometric and dynamic similarity in the hydrology (e.g. matching heap geometry, irrigation conditions, and Peclet and capillary numbers) leads to similar dimensionless RTDs in geometrically similar heaps. For heaps that exhibit dual-porosity behaviour, we introduced additional dimensionless parameters—a capacity ratio between mobile and immobile liquid domains and an interporosity Damköhler number  $\text{Da}_{\text{ex}}$ —which together control how rapidly reagent in advective channels can

access the reactive matrix. These parameters naturally complement the dimensionless groups used in more detailed dual-porosity heap models reported in the hydrometallurgical literature [Robertson, 2017, Miao et al., 2017, 2021, Blackmore et al., 2018, Dixon et al., 2021].

At the microscopic level, we used the shrinking-core model to derive explicit expressions for how a PSD in particle diameter maps into distributions of Damköhler numbers under external film control, intraparticle diffusion control, and mixed control. These formulas make quantitatively clear that:

- For film-controlled systems, the relevant Damköhler number scales as  $d_p^{-1}$ , so coarsening the PSD penalises leaching rates, but the sensitivity is moderate.
- For diffusion-controlled systems, the Damköhler number scales as  $d_p^{-2}$ , leading to a much stronger dependence on PSD tails and a heavy-tailed distribution of particle-scale Damköhler numbers.
- In mixed-control systems, each particle is characterised by a pair of Damköhler numbers (for film and diffusion) or an effective Damköhler number and a resistance ratio. The PSD therefore induces a one-dimensional curve in this two-dimensional parameter space, and the impact of changing the PSD depends on how this curve spans regions of film-, diffusion- and mixed-control behaviour.

Simple numerical examples were used to illustrate these points. For a lognormal PSD with parameters typical of crushed ore, the diffusion-controlled Damköhler distribution was found to be considerably more skewed than the film-controlled distribution, with the smallest particles exerting a disproportionate influence on the mean Damköhler number. An illustrative heap example showed how fine and coarse PSDs produce markedly different heap-averaged conversion trajectories under both mechanisms, with diffusion-controlled systems exhibiting higher conversions but also larger absolute penalties when the PSD is coarsened.

From a practical standpoint, the analysis suggests several implications for hydrometallurgical heap leaching:

- Matching only macroscopic hydraulic conditions (e.g. irrigation rate, solution chemistry, overall RTD) between column tests and full-scale heaps is not sufficient for predictive scale-up if the PSD and dual-porosity structure differ significantly.
- Laboratory testwork intended to support design of industrial heaps should, where possible, preserve not only the PSD but also the key dual-porosity parameters (mobile/immobile capacity ratio, interporosity exchange rate) and operating regimes that determine whether film, diffusion or mixed control is dominant.
- The dimensionless groups identified here provide a compact way to document and compare column and heap conditions, to assess whether two systems are “similar enough” for direct transfer of kinetic information, and to design sensitivity studies on PSD and ore type.

The present framework could be extended in several directions of interest for future work: coupling to microbially mediated kinetics in bioleaching, incorporating more general intraparticle reaction–diffusion models or multi-mineral ore textures, and embedding the dimensionless structure into existing numerical simulators such as HeapSim or dual-porosity flow codes for parameter screening and model reduction. Ultimately, we hope that expressing heap leaching in terms of a small set of well-defined dimensionless groups will aid practitioners in designing more informative testwork, in understanding the impact of PSD and ore variability, and in achieving more robust and transparent scale-up in hydrometallurgical heap operations.

## Nomenclature (dimensional parameters)

### Geometry and hydrodynamics

$H$	heap (or column) height [m]
$z$	vertical coordinate [m]
$V$	reactor/heap control volume [ $\text{m}^3$ ]
$q$	superficial liquid flux [ $\text{m s}^{-1}$ ]
$u$	interstitial velocity, $u = q/\varepsilon$ [ $\text{m s}^{-1}$ ]
$\tau_{\text{heap}}$	advective time scale, $\varepsilon H/q$ [s]
$D_{\text{ax}}$	effective axial dispersion coefficient [ $\text{m}^2 \text{ s}^{-1}$ ]
$D_{\text{ax},m}$	axial dispersion in mobile domain [ $\text{m}^2 \text{ s}^{-1}$ ]

## Solid and particle-scale transport

$d_p$	particle diameter [m]
$R_0$	initial particle radius ( $d_p/2$ ) [m]
$\rho_s$	solid density [ $\text{kg m}^{-3}$ ]
$D_{\text{eff}}$	effective diffusivity in product layer [ $\text{m}^2 \text{ s}^{-1}$ ]
$k_f$	external mass-transfer coefficient [ $\text{m s}^{-1}$ ]

## Chemistry and dual porosity

$C_\infty$	bulk reagent concentration [ $\text{mol m}^{-3}$ ]
$C_m, C_{im}$	mobile and immobile concentrations [ $\text{mol m}^{-3}$ ]
$\alpha$	mobile–immobile exchange coefficient [ $\text{s}^{-1}$ ]
$\varepsilon$	total porosity [-]
$\varepsilon_m, \varepsilon_{im}$	mobile/immobile porosities [-]

## Acknowledgements

[Text omitted.]

## References

O. Levenspiel. *Chemical Reaction Engineering*, 3rd ed. Wiley, New York, 1999.

H. S. Fogler. *Elements of Chemical Reaction Engineering*, 5th ed. Prentice Hall, Upper Saddle River, NJ, 2016.

H. S. Fogler. The shrinking core model. In *Elements of Chemical Reaction Engineering*, 4th ed. Expanded material, University of Michigan, 2005.

J. Szekely, J. W. Evans, and H. Y. Sohn. *Gas–Solid Reactions*. Academic Press, New York, 1975.

J. W. Evans and H. Y. Sohn. Gas–solid reactions. In *Treatise on Process Metallurgy*, vol. 2, pp. 437–482. Elsevier, 2011.

M. C. Fuerstenau. Shrinking core models in hydrometallurgy: What students are not being told. *Hydrometallurgy*, 79(1–2):23–30, 2005.

C. Moreno-Pulido, R. Olwande, T. Myers, and F. Font. Approximate solutions to the shrinking core model. *arXiv preprint*, arXiv:2507.21042, 2025.

D. G. Dixon. Investigative study into the hydrodynamics of heap leaching processes. Technical report, University of Cape Town, 2003.

D. McBride, N. Croft, and M. Cross. Preferential flow behaviour in unsaturated packed beds and heaps. *Hydrometallurgy*, 165:1–16, 2016.

D. Rodrigues, J. Petersen, and D. G. Dixon. Residence time distribution analysis of drip-irrigated beds characteristic of heap leaching. *Minerals*, 13(2):267, 2023.

D. G. Dixon and J. Petersen. Comprehensive modelling study of chalcocite column and heap bioleaching. In P. A. Riveros, D. G. Dixon, D. B. Dreisinger, and J. Menacho (eds.), *Hydrometallurgy of Copper (Copper 2003)*, vol. 6, pp. 493–516. CIM, Montreal, 2003.

D. G. Dixon and J. Petersen. Modeling the dynamics of heap bioleaching for process improvement and innovation. In *Hydro-Sulfides 2004: Proceedings of the International Colloquium on Hydrometallurgical Processing of Copper Sulfides*, pp. 13–45, 2004.

D. G. Dixon, J. Petersen, et al. Towards fundamentally based heap leaching scale-up. *Hydrometallurgy*, 199:105512, 2021.

H. ElGhamrawy, D. G. Dixon, and J. Petersen. HeapSim2D—A 2D axisymmetric model of heap leaching under drip irrigation. *Hydrometallurgy*, 208:105725, 2022.

S. Robertson. Development of an integrated heap leach solution flow and mineral leaching model. *Hydrometallurgy*, 169:79–88, 2017.

X. Miao, G. Narsilio, A. Wu, and B. Yang. A 3D dual pore-system leaching model. Part 1: Study on fluid flow. *Hydrometallurgy*, 167:173–182, 2017.

X. Miao, A. Wu, B. Yang, and G. Narsilio. Development of a 3D dual pore-system leaching model: Application on metal extraction from oxide copper ore. *International Journal of Heat and Mass Transfer*, 169:120895, 2021.

S. Blackmore, D. Pedretti, K. U. Mayer, L. Smith, and R. D. Beckie. Evaluation of single- and dual-porosity models for reproducing the release of external and internal tracers from heterogeneous waste-rock piles. *Journal of Contaminant Hydrology*, 214:65–74, 2018.

G. A. Sheikhzadeh, M. A. Mehrabian, S. H. Mansouri, and A. Sarrafi. Computational modelling of unsaturated flow of liquid in heap leaching—using the results of column tests to calibrate the model. *International Journal of Heat and Mass Transfer*, 48:279–292, 2005.

G. I. Barenblatt, I. P. Zheltov, and I. N. Kochina. Basic concepts in the theory of seepage of homogeneous liquids in fissured rocks [strata]. *Journal of Applied Mathematics and Mechanics*, 24:1286–1303, 1960.

J. E. Warren and P. J. Root. The behavior of naturally fractured reservoirs. *Society of Petroleum Engineers Journal*, 3(3):245–255, 1963.

R. W. Zimmerman, G. Chen, and G. S. Bodvarsson. A dual-porosity model with semianalytical treatment of fracture/matrix flow. *Water Resources Research*, 29(7):2127–2137, 1993.

U. Dogru and K. Pruess. Modeling flow in porous media with double porosity/permeability approaches. *Transport in Porous Media*, 135:1–28, 2020.

C. Moreno-Pulido, R. Olwande, T. Myers, and F. Font. Approximate analytical solutions for the shrinking core model and their interpretation. *Preprint*, 2023.